Crystal Structure of the Catalytic Domain of MCR-1 (cMCR-1) in Complex with D-Xylose

Zhao-Xin Liu [1,2,†], Zhenggang Han [1,†], Xiao-Li Yu [1], Guoyuan Wen [3] and Chi Zeng [1,3,*]

[1] Hubei Province Engineering Research Center of Healthy Food, School of Biology and Pharmaceutical Engineering, Wuhan Polytechnic University, Wuhan 430023, China; jiangxinklzx@163.com (Z.-X.L.); zhengganghan@whpu.edu.cn (Z.H.); yxll268@126.com (X.-L.Y.)
[2] College of Life Sciences, Wuhan University, Wuhan 430072, China
[3] Key Laboratory of Prevention and Control Agents for Animal Bacteriosis (Ministry of Agriculture), Institute of Animal Husbandry and Veterinary, Hubei Academy of Agricultural Sciences, Wuhan 430064, China; wgy_524@163.com
* Correspondence: czeng@whpu.edu.cn
† These authors contributed equally to this work.

check for updates

Abstract: The polymyxin colistin is known as a "last resort" antibacterial drug toward pandrug-resistant enterobacteria. The recently discovered plasmid-encoded *mcr-1* gene spreads rapidly across pathogenic strains and confers resistance to colistin, which has emerged as a global threat. The *mcr-1* gene encodes a phosphoethanolamine transferase (MCR-1) that catalyzes the transference of phosphoethanolamine to lipid A moiety of lipopolysaccharide, resulting in resistance to colistin. Development of effective MCR-1 inhibitors is crucial for combating MCR-1-mediated colistin resistance. In this study, MCR-1 catalytic domain (namely cMCR-1) was expressed and co-crystallized together with D-xylose. X-ray crystallographic study at a resolution of 1.8 Å found that cMCR-1-D-xylose co-crystals fell under space group $P2_12_12_1$, with unit-cell parameters a = 51.6 Å, b = 73.1 Å, c = 82.2 Å, α = 90°, β = 90°, γ = 90°. The asymmetric unit contained a single cMCR-1 molecule complexed with D-xylose and had a solvent content of 29.13%. The structural model of cMCR-1-D-xylose complex showed that a D-xylose molecule bound in the putative lipid A-binding pocket of cMCR-1, which might provide a clue for MCR-1 inhibitor development.

Keywords: polymyxin resistance; colistin resistance; MCR-1

1. Introduction

Antimicrobial resistance among Gram-negative bacteria, especially the multidrug-resistant enterobacteria which are the leading cause of human clinical infections, is a global healthcare concern [1]. The carbapenemase-producing carbapenem-resistant *Enterobacteriaceae* (CRE), such as *Klebsiella pneumoniae* strains expressing the KPC-2 enzyme and *Enterobacteriaceae* strains expressing the NDM-1 enzyme, are of special clinical importance [1].

Polymyxin is often employed as the final therapeutic option to treat CRE-caused clinical infections because of its low resistance and high efficiency among CRE [2]. Polymyxins (colistin, polymyxin B) are cationic polypeptides which could bind the lipid A moiety of bacterial lipopolysaccharide and disrupt the bacterial cytomembrane subsequently [2]. Bacterial polymyxin resistance was considered to be very low and primarily caused by genomic mutations associated with specific two-component regulatory systems, which either modify lipid A or lead to complete loss of the lipopolysaccharide [2].

Recently, a novel mobile colistin resistance mechanism, led by a protein named MCR-1 (a phosphoethanolamine (PEA) transferase that confers colistin resistance by catalyzing the transference

of phosphoethanolamine to lipid A moiety of lipopolysaccharide), has been discovered [3]. The gene encoding MCR-1 (*mcr-1*) has been shown plasmid-located and self-transmittable between various bacterial strains [2]. Until now, *mcr-1* has already been detected within a broad range of pathogenic isolates from humans and animals worldwide, which poses a huge threat to the sustaining effectiveness of colistin against CRE-caused clinical infections [2]. Development of effective MCR-1 inhibitors might be the only way to extend the usage of colistin as a reserved antibacterial drug to treat CRE infections [4].

Although several structures of MCR-1 catalytic domain (namely cMCR-1) have been determined [5–8], few effective inhibitors for MCR-1 are known. A recent co-crystallization study [9] showed that two substrate analogues of MCR-1, ethanolamine and D-glucose, could specifically bind to cMCR-1. Here, the crystallization and primary structure analysis of cMCR-1 complexed with D-xylose is reported. The structure determined showed that a D-xylose molecule bound in the putative lipid A-binding pocket of cMCR-1, which might provide a clue for MCR-1 inhibitor development.

2. Materials and Methods

2.1. Recombinant cMCR-1 Production

The sequence of *mcr-1* gene is available in GenBank (GenBank accession no. KY685070). Based on the secondary structure predictions, the MCR-1 catalytic domain (namely cMCR-1) includes 326 amino acids, from Pro216 to Arg541. The partial *mcr-1* gene sequence encoding cMCR-1 with *Nco*I/*Xho*I restriction sites incorporated at the 5′/3′ ends was commercially synthesized and cloned into *Nco*I/*Xho*I restriction sites of the expression vector pET-28a(+) (Novagen), creating pET-28a(+)-mcr-1. In construct pET-28a(+)-mcr-1, a histidine tag (HHHHHH) was fused to the C-terminus of cMCR-1 (Table 1).

Table 1. Production specifics for cMCR-1.

Source	*Escherichia coli*
DNA	Synthesized DNA
Forward primer [1]	5′-CATG<u>CCATGG</u>CCAAAAGATACCATTTATCAC-3′
Reverse primer [2]	5′-CC<u>CTCGAG</u>GCGGATGAATGCGGTGCGGTC-3′
Expression vector	pET-28a(+)
Host	*E. coli* BL21(DE3)pLysS
Recombinant protein sequence [3]	<u>MG</u>PKDTIYHAKDAVQATKPDMRKPRLVVF VVGETARADHVSFNGYERDTFPQLAKIDGVTNF SNVTSCGTSTAYSVPCMFSYLGADEYDVDTAK YQENVLDTLDRLGVSILWRDNNSDSKGVMDKLPKA QFADYKSATNNAICNTNPYNECRDVGMLVGLDDFV AANNGKDMLIMLHQMGNHGPAYFKRYDEKFAKFT PVCEGNELAKCEHQSLINAYDNALLATDDFIAQSIQ WLQTHSNAYDVSMLYVSDHGESLGENGVYLHGMP NAFAPKEQRSVPAFFWTDKQTGITPMATDTVLTHD AITPTLLKLFDVTADKVKDRTAFIR<u>LEHHHHHH</u>

[1] The *Nco*I site noted. [2] The *Xho*I site noted. [3] The cloning artifacts are underlined.

Escherichia coli BL21(DE3)pLysS was transformed with pET-28a(+)-mcr-1 and grown at 310 K, 200 rpm rotation in LB liquid medium containing 50 μg mL^{-1} kanamycin for cMCR-1 expression. Confluent cultures (OD$_{600}$~0.6) were then treated with 0.3 mM (final concentration) IPTG at 298 K with shaking (180 rpm) for 20 h. Cells were collected by 20 min of centrifugation (4500 g, 277 K) and pellets were kept at 193 K for subsequent use.

The cell pellets were lysed with 10 mM Tris-HCl pH 8.0, 200 mM NaCl, 5% (*v/v*) glycerol, 0.3% (*v/v*) Triton X-100, 1 mM DTT, and 0.1 mM PMSF in a French press. Cell wastes were excluded by

centrifuging the lysates at 12,000 g for 30 min at 277 K, and the supernatant was clarified using a 0.45 μm filter and then passed through a pre-equilibrated Ni-NTA affinity column (GE Healthcare). The affinity column was washed thoroughly using 10 mM Tris-HCl pH 8.0 containing 50 mM imidazole to remove the miscellaneous proteins. The target proteins were eluted using 10 mM Tris-HCl pH 8.0 containing 200 mM imidazole. Concentrated protein was then loaded onto a MonoQ 5/50 GL anion exchange column (GE Healthcare) and chromatographed at 1 mL min^{-1} using a linear NaCl gradient generated with 10 mM Tris-HCl pH 8.0 (buffer A) and 10 mM Tris-HCl pH 8.0, 1 M NaCl (buffer B). Peak fractions were pooled and run through a Superdex 200 10/300 GL column (GE Healthcare) equilibrated with buffer A at a flow rate of 1 mL min^{-1}. Peak fractions were recovered and concentrated to 10 mg mL^{-1} for crystallization. The purity of the final protein (cMCR-1) was checked by SDS-PAGE. All specifics for recombinant cMCR-1 production are present in Table 1.

2.2. Crystallization

The cMCR-1 was crystallized at 277 K using the sitting-drop vapor-diffusion method as described by Wei et al. [9]. The 0.5 μL sitting drops consisting of 0.25 μL cMCR-1 solution and 0.25 μL reservoir solution were equilibrated against 30 μL reservoir solution in 96-well MRC plates (Molecular Dimensions). The best crystals were achieved in 10% (*w/v*) PEG 1000, 5% (*w/v*) PEG 8000.

2.3. Data Collection, Structure Solution, and Refinement

The cMCR-1 crystals were incubated in mother liquor containing 100 mM D-xylose for 10 s to form the cMCR-1-D-xylose complex. The cMCR-1-D-xylose co-crystals used for diffraction data collection were incubated in cryoprotectant (mother liquor containing 20% (*v/v*) glycerol) for 10 s before flash cooling in streams of liquid nitrogen. Data for cMCR-1-D-xylose complex were acquired at 100 K using an ADSC Q315r detector at beamline BL17U1 of Shanghai Synchrotron Radiation Facility (SSRF), China; 360 frames were taken with 1.0° oscillations. The data were indexed, integrated, and scaled using *HKL-2000* (HKL Research, Inc., Charlottesville, VA, USA) [10] and *iMosflm* programs [11]. The structure was solved by molecular replacement with *Phaser* [12] using a single monomer of cMCR-1 (PDB entry 5GRR [7]) as the search model. The structure model was constructed using alternating manual building in *Coot* [13] and restrained refinement in *PHENIX* [14]. The final model was optimized on PDB_REDO web server [15] and validated by *MolProbity* [16]. All figures were prepared by *PyMOL* (Schrödinger). Table 2 summarizes data-collection and crystallographic statistics of cMCR-1-D-xylose complex. Coordinates and structure factors of the cMCR-1-D-xylose complex have been deposited in the Protein Data Bank (PDB) under accession code 5ZJV.

Table 2. Data-collection and crystallographic statistics of cMCR-1-D-xylose complex.

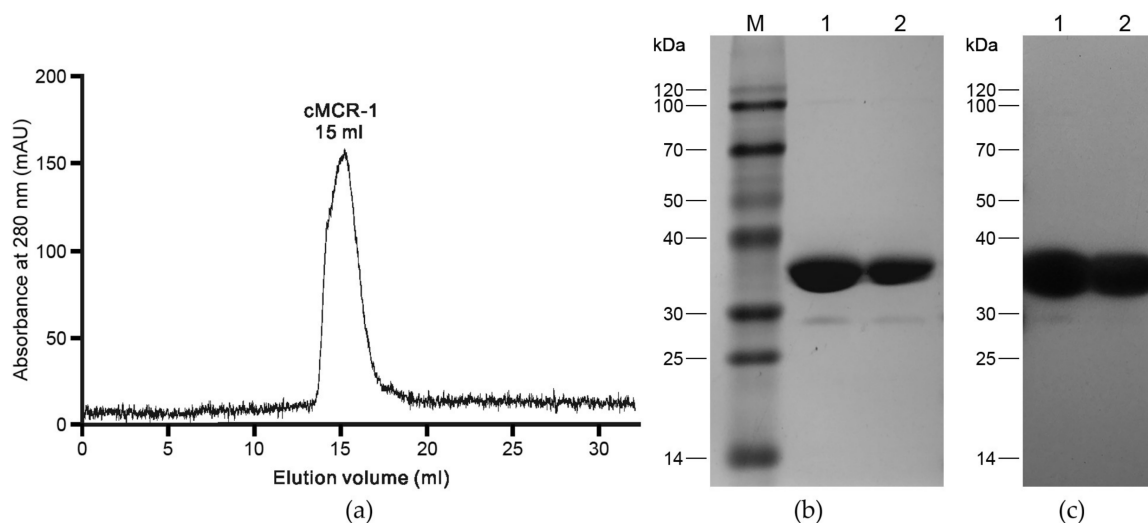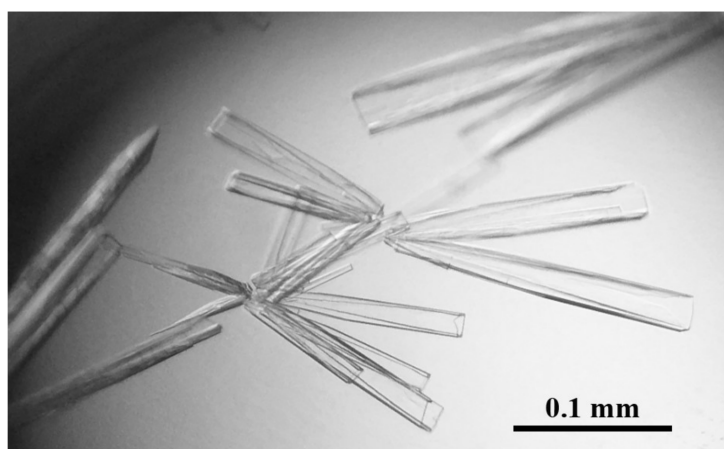| Diffraction Source	BL17U1, SSRF
Wavelength (Å)	0.9792
Temperature (K)	100
Detector	ADSC Q315r
Crystal-to-detector distance (mm)	350
Total rotation range (°)	360
Rotation range per image (°)	1.0
Exposure time per image (s)	0.5
Space group	$P2_12_12_1$
a, b, c (Å)	51.6, 73.1, 82.2
α, β, γ (°)	90, 90, 90
Resolution range (Å)	43.71–1.82 (1.88–1.82) [1]
Total number of reflections	56014 (5514)
Number of unique reflections	28258 (2789)
Mosaicity (°)	0.5
Multiplicity	2.0 (2.0)
Completeness (%)	99.0 (99.0)
Mean $I/\sigma(I)$	10.61 (4.94)
R_{merge} (%)	3.5 (11.1)
$CC_{1/2}$	0.997 (0.949)
Wilson plot overall B factor (Å^2)	13.74
Reflection number, working set	28223 (2785)
Reflection number, test set	1997 (196)
R_{work}	0.139
R_{free}	0.178
Ramachandran favored region (%)	98
Ramachandran allowed region (%)	1.75
Ramachandran outliers (%)	0.25
Rotamer outliers (%)	0.65
R.m.s.d. bond lengths (Å)	0.006
R.m.s.d. bond angles (°)	0.86
Average B factor (Å^2)	17.55

[1] Outer shell values.

3. Results and Discussion

As stated in the Introduction, development of effective MCR-1 inhibitors is crucial for combating the threat of colistin resistance mediated by MCR-1. A recent co-crystallization study [9] showed that two substrate analogues of MCR-1 (ethanolamine and D-glucose) could specifically bind to MCR-1 catalytic domain (cMCR-1). Both D-glucose and lipid A are hexacyclic compounds. Thus, we tried many other hexacyclic compounds for co-crystallization with cMCR-1 (unpublished). The only other co-crystal structure was that obtained for the complex formed between cMCR-1 and D-xylose at a resolution of 1.8 Å.

MCR-1 belongs to the phosphoethanolamine (PEA) transferase family. It contains 541 amino acids with an N-terminal five-helix transmembrane domain (amino acid residues 1–215) and a C-terminal periplasmic catalytic domain (amino acid residues 216–541) [9]. In order to investigate the potential interactions between D-xylose (and other hexacyclic compounds) and MCR-1, cMCR-1 (MCR-1 catalytic domain) was expressed and purified using a combine of affinity, anion exchange and gel filtration chromatography (Figure 1a), as stated in Section 2.1. The purity of the purified cMCR-1 was confirmed with SDS-PAGE (Figure 1b) and subsequent Western blot analysis (Figure 1c). The cMCR-1 was effectively crystallized using the sitting-drop vapor-diffusion method as described by Wei et al. [9], which generated diffraction-quality crystals with a longest dimension of 0.2 mm (Figure 2). SDS-PAGE showed that the obtained crystals were protein crystals and had the same molecular weight as the

purified cMCR-1 protein (Figure 1b). The cMCR-1 crystals were incubated in the mother liquor supplemented with 100 mM D-xylose for 10 s to form the cMCR-1-D-xylose complex.
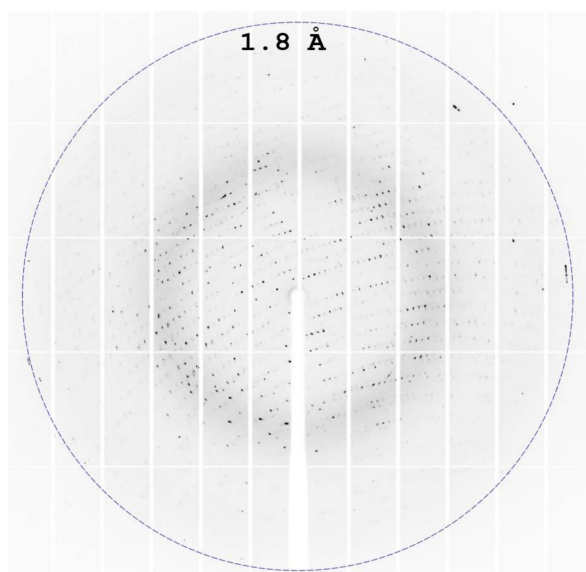

Figure 1. Purification and purity analysis of cMCR-1. (**a**) Gel filtration chromatography of cMCR-1. (**b**) SDS-PAGE of the final purified cMCR-1 and cMCR-1 crystals. Molecular-weight markers (lane M, labelled in kDa), purified ~35 kDa cMCR-1 protein (lane 1) and cMCR-1 crystals (lane 2) are shown. (**c**) Western blot analysis of the final purified cMCR-1 and cMCR-1 crystals using an anti-6×His antibody. Purified ~35 kDa cMCR-1 protein (lane 1) and cMCR-1 crystals (lane 2) are shown.
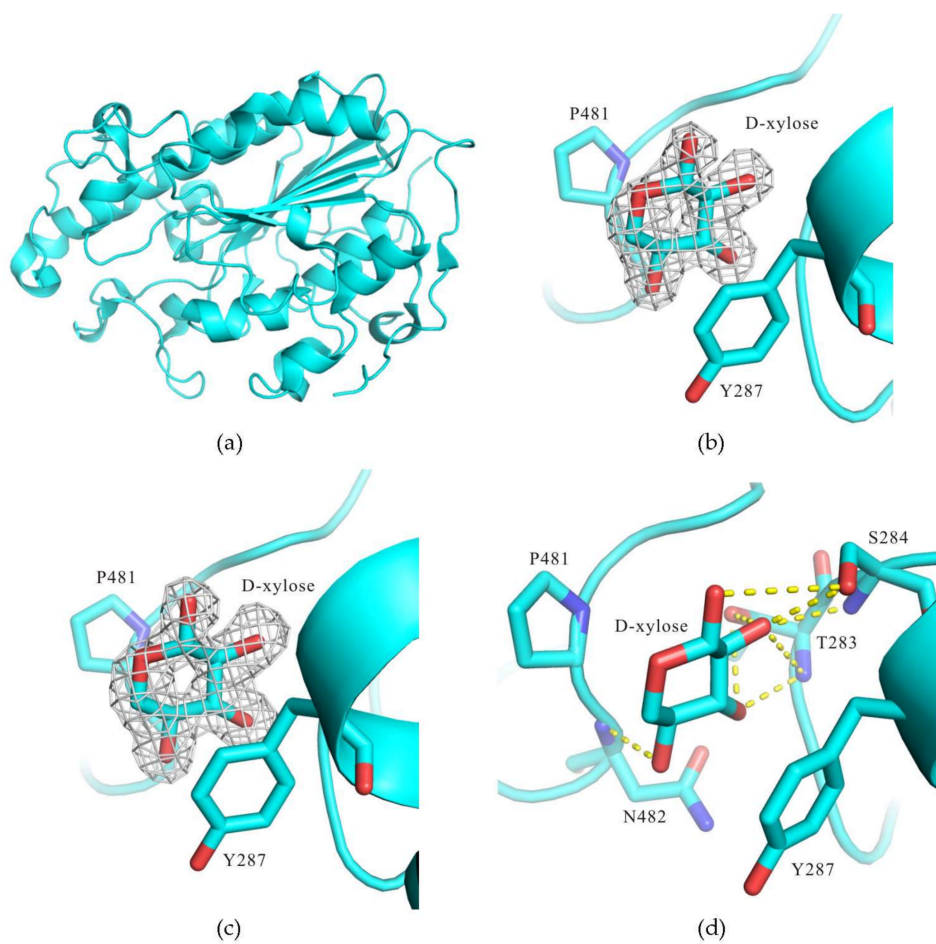

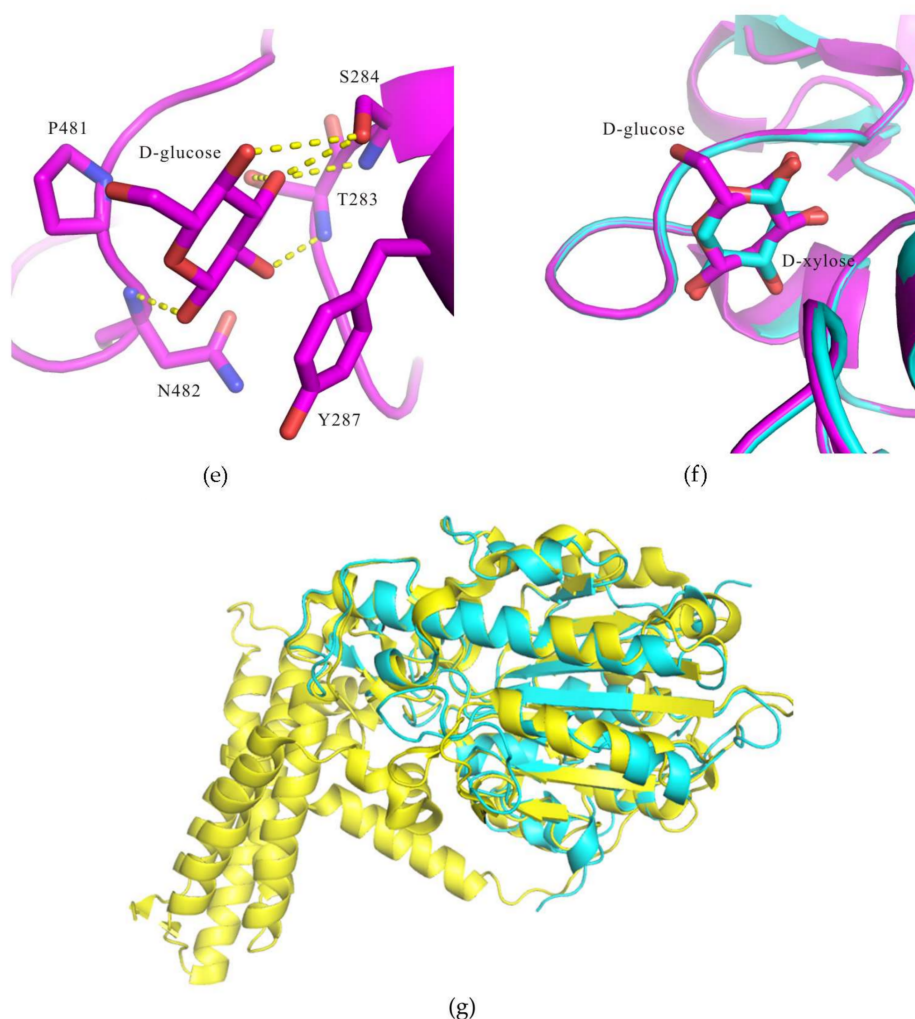**Figure 2.** Crystals of cMCR-1.

Diffraction data for the cMCR-1-D-xylose complex was collected to 1.8 Å resolution (Figure 3) and on its basis, the cMCR-1-D-xylose co-crystals fell under space group $P2_12_12_1$, possessing unit-cell parameters $a = 51.6$ Å, $b = 73.1$ Å, $c = 82.2$ Å, $\alpha = 90°$, $\beta = 90°$, $\gamma = 90°$. The asymmetric unit contained a single cMCR-1 molecule complexed with D-xylose. The data set of X-ray diffraction had a resolution range from 43.71 Å to 1.82 Å with 3.5% R_{merge} and 99.0% completeness. To elucidate the structure of cMCR-1-D-xylose complex, we employed molecular replacement method using cMCR-1 monomer (PDB entry 5GRR [7]) as a search model and obtained a clear solution. We confirmed the occurrence of a single protein molecule in the asymmetric unit by cross-rotation and translation-function calculations; the corresponding solvent content was 29.13%. Initial structure refinement using *PHENIX* [14] yielded a model (Figure 4a) with an R_{work} of 13.9% and an R_{free} of 17.8%.

Figure 3. Representative X-ray diffraction pattern of cMCR-1-D-xylose co-crystal.

(a)

(b)

(c)

(d)

Figure 4. *Cont.*

(e)

(f)

(g)

Figure 4. Structure of the cMCR-1-D-xylose complex. (**a**) The ribbon diagram showing the overall structure of cMCR-1. (**b**) The Fo-Fc electron-density map contoured at 3.0 σ depicting the D-xylose molecule. The map was calculated using the model omitting the D-xylose molecule after rounds of refinement. (**c**) The 2Fo-Fc electron-density map contoured at 1.0 σ depicting the D-xylose molecule. (**d**) Interaction between cMCR-1 and the D-xylose molecule. (**e**) Interaction between cMCR-1 and the D-glucose molecule. (**f**) Superposition of cMCR-1-D-xylose (cyan) and cMCR-1-D-glucose (magenta). (**g**) Superposition of cMCR-1-D-xylose (cyan) and EptA (yellow). All figures were prepared using *PyMOL* (Schrödinger).

As shown in the Fo-Fc map (contoured at 3.0 σ level) (Figure 4b) and 2Fo-Fc map (contoured at 1.0 σ level) (Figure 4c), a D-xylose molecule bound in the putative lipid A-binding pocket of cMCR-1. According to the PDB structure validation report, real space correlation coefficient (RSCC) and real space r-value (RSR) are 0.94 and 0.13, respectively, for the ligand D-xylose. The D-xylose, Pro481, and Tyr287 formed a sandwich structure with the D-xylose molecule in the middle (Figure 4d). Obviously, the hydrophobic stacking interaction played a crucial role in D-xylose recognition.

The structure of cMCR-1-D-xylose complex is similar with that of cMCR-1-D-glucose complex (PDB entry 5YLF [9]). Meanwhile, there are still many differences between the two structures. First, alignment of the two structures (Figure 4f) showed that both D-xylose and D-glucose bound to the same pocket of cMCR-1 and formed a π-π-conjugated interaction with Pro481 and Tyr287 of cMCR-1, but the skeletons of D-xylose and D-glucose were in the opposite positions. Next, we analyzed the cMCR-1-D-xylose and cMCR-1-D-glucose interactions by using

PISA server (http://www.ebi.ac.uk/pdbe/pisa). The accessible surface area (ASA) = 269.67 Å^2, buried surface area (BSA) = 194.27 Å^2, solvation energy effect (Δ^iG) = −2.37 kcal/mol between D-xylose and cMCR-1, and the ASA = 303.17 Å^2, BSA = 204.82 Å^2, Δ^iG = −2.97 kcal/mol between D-glucose and cMCR-1. It suggested that the interaction between D-glucose and cMCR-1 is greater than that between D-xylose and cMCR-1. The D-xylose and D-glucose molecules also bound to cMCR-1 through a large number of hydrogen bonds. The O1, O2, O3, and O4 atoms of D-xylose hydrogen-bonded to Ser284 OG, Thr283 OG1, N/Ser284 N, OG, Thr283 OG1, N, and Asn482 N, respectively (Figure 4d). The O1, O2, O3, and O4 atoms of D-glucose hydrogen-bonded to Asn482 N, Thr283 N, Ser284 N, OG/Thr283 OG1, and Ser284 OG, respectively (Figure 4e).

We also conducted a comparison of cMCR-1-D-xylose complex with phosphoethanolamine transferase A (EptA) from *Neisseria meningitides* (PDB entry 5FGN [17]), the only structure of a full-length phosphoethanolamine transferase so far. The structure of cMCR-1-D-xylose complex can be well superimposed with the structure of EptA catalytic domain, with a Cα root-mean-square deviation of 2.0 Å as revealed by Dali server (http://ekhidna.biocenter.helsinki.fi/dali_server/start) [18] (Figure 4g). Anandan et al. [17] have shown that detergent dodecyl-β-D-maltoside (DDM) could bind in a substrate pocket of EptA, and the pocket bound by DDM was probably the phosphoethanolamine (PEA) binding pocket near the putative lipid A-binding pocket.

In conclusion, our finding that D-xylose could bind in the putative lipid A-binding pocket of cMCR-1 is interesting, which might provide a clue for MCR-1 inhibitor development. In vitro inhibitory assay is currently in progress to confirm if D-xylose could inhibit colistin resistance mediated by MCR-1.

Author Contributions: Zhao-Xin Liu and Chi Zeng designed the experiments. Zhao-Xin Liu performed the experiments. Zhao-Xin Liu, Chi Zeng, and Zhenggang Han analyzed the data. Xiao-Li Yu and Guoyuan Wen provided technical support. Zhao-Xin Liu, Chi Zeng, and Zhenggang Han completed the paper.

Conflicts of Interest: No interest conflict exists among the authors.

References

1. Logan, L.K.; Weinstein, R.A. The epidemiology of carbapenem-resistant *Enterobacteriaceae*: The impact and evolution of a global menace. *J. Infect. Dis.* **2017**, *215*, S28–S36. [CrossRef] [PubMed]

2. Poirel, L.; Jayol, A.; Nordmann, P. Polymyxins: Antibacterial activity, susceptibility testing, and resistance mechanisms encoded by plasmids or chromosomes. *Clin. Microbiol. Rev.* **2017**, *30*, 557–596. [CrossRef] [PubMed]

3. Liu, Y.Y.; Wang, Y.; Walsh, T.R.; Yi, L.X.; Zhang, R.; Spencer, J.; Doi, Y.; Tian, G.; Dong, B.; Huang, X.; et al. Emergence of plasmid-mediated colistin resistance mechanism MCR-1 in animals and human beings in China: A microbiological and molecular biological study. *Lancet Infect. Dis.* **2016**, *16*, 161–168. [CrossRef]

4. Hu, Y.Y.; Wang, Y.L.; Sun, Q.L.; Huang, Z.X.; Wang, H.Y.; Zhang, R.; Chen, G.X. Colistin resistance gene *mcr-1* in gut flora of children. *Int. J. Antimicrob. Agents* **2017**, *50*, 593–597. [CrossRef] [PubMed]

5. Hinchliffe, P.; Yang, Q.E.; Portal, E.; Young, T.; Li, H.; Tooke, C.L.; Carvalho, M.J.; Paterson, N.G.; Brem, J.; Niumsup, P.R.; et al. Insights into the mechanistic basis of plasmid-mediated colistin resistance from crystal structures of the catalytic domain of MCR-1. *Sci. Rep.* **2017**, *7*, 39392. [CrossRef] [PubMed]

6. Hu, M.; Guo, J.; Cheng, Q.; Yang, Z.; Chan, E.W.C.; Chen, S.; Hao, Q. Crystal structure of *Escherichia coli* originated MCR-1, a phosphoethanolamine transferase for colistin resistance. *Sci. Rep.* **2016**, *6*, 38793. [CrossRef] [PubMed]

7. Ma, G.; Zhu, Y.; Yu, Z.; Ahmad, A.; Zhang, H. High resolution crystal structure of the catalytic domain of MCR-1. *Sci. Rep.* **2016**, *6*, 39540. [CrossRef] [PubMed]

8. Stojanoski, V.; Sankaran, B.; Prasad, B.V.; Poirel, L.; Nordmann, P.; Palzkill, T. Structure of the catalytic domain of the colistin resistance enzyme MCR-1. *BMC Biol.* **2016**, *14*, 81. [CrossRef] [PubMed]

9. Wei, P.; Song, G.; Shi, M.; Zhou, Y.; Liu, Y.; Lei, J.; Chen, P.; Yin, L. Substrate analog interaction with MCR-1 offers insight into the rising threat of the plasmid-mediated transferable colistin resistance. *FASEB J.* **2018**, *32*, 1085–1098. [CrossRef] [PubMed]

10. Otwinowski, Z.; Minor, W. Processing of X-ray diffraction data collected in oscillation mode. *Methods Enzymol.* **1997**, *276*, 307–326. [CrossRef] [PubMed]

11. Battye, T.G.; Kontogiannis, L.; Johnson, O.; Powell, H.R.; Leslie, A.G. *iMOSFLM*: A new graphical interface for diffraction-image processing with *MOSFLM*. *Acta Crystallogr. D Biol. Crystallogr.* **2011**, *67*, 271–281. [CrossRef] [PubMed]

12. McCoy, A.J.; Grosse-Kunstleve, R.W.; Adams, P.D.; Winn, M.D.; Storoni, L.C.; Read, R.J. *Phaser* crystallographic software. *J. Appl. Crystallogr.* **2007**, *40*, 658–674. [CrossRef] [PubMed]

13. Emsley, P.; Cowtan, K. *Coot*: Model-building tools for molecular graphics. *Acta Crystallogr. D Biol. Crystallogr.* **2004**, *60*, 2126–2132. [CrossRef] [PubMed]

14. Adams, P.D.; Afonine, P.V.; Bunkóczi, G.; Chen, V.B.; Davis, I.W.; Echols, N.; Headd, J.J.; Hung, L.W.; Kapral, G.J.; Grosse-Kunstleve, R.W.; et al. *PHENIX*: A comprehensive Python-based system for macromolecular structure solution. *Acta Crystallogr. D Biol. Crystallogr.* **2010**, *66*, 213–221. [CrossRef] [PubMed]

15. Joosten, R.P.; Long, F.; Murshudov, G.N.; Perrakis, A. The PDB_REDO server for macromolecular structure model optimization. *IUCrJ* **2014**, *1*, 213–220. [CrossRef] [PubMed]

16. Chen, V.B.; Arendall, W.B.; Headd, J.J.; Keedy, D.A.; Immormino, R.M.; Kapral, G.J.; Murray, L.W.; Richardson, J.S.; Richardson, D.C. *MolProbity*: All-atom structure validation for macromolecular crystallography. *Acta Crystallogr. D Biol. Crystallogr.* **2010**, *66*, 12–21. [CrossRef] [PubMed]

17. Anandan, A.; Evans, G.L.; Condic-Jurkic, K.; O'Mara, M.L.; John, C.M.; Phillips, N.J.; Jarvis, G.A.; Wills, S.S.; Stubbs, K.A.; Moraes, I.; et al. Structure of a lipid A phosphoethanolamine transferase suggests how conformational changes govern substrate binding. *Proc. Natl. Acad. Sci. USA* **2017**, *114*, 2218–2223. [CrossRef] [PubMed]

18. Holm, L.; Laakso, L.M. Dali server update. *Nucleic Acids Res.* **2016**, *44*, W351–W355. [CrossRef] [PubMed]